International Journal of
Mathematical Modelling & Computations
Vol. 04, No. 04, Fall 2014, 389- 400

Spot Patterns in Gray Scott Model with Application to Epidemic Control

Muhammad, A. Yau[a,*] , M. U. Adehi [b] and Muktari Garba[c]

[a,b] *Department of Mathematical Sciences, Nasarawa State University Keffi, Nigeria*;
[c] *Department of Statistics, Waziri Umaru Federal Polytechnic Birnin-Kebbi, Nigeria.*

Abstract. In this work, we analyse a pair of two-dimensional coupled reaction-diffusion equations known as the Gray-Scott model, in which spot patterns have been observed. We focus on stationary patterns, and begin by deriving the asymptotic scaling of the parameters and variables necessary for the analysis of these patterns. A complete numerical study of the system is presented. We use backward Euler and Crank-Nicolson methods to study the model 1. We compute the error in L^2 and L^∞ norms and also the EOCS are calculated for each method. The errors and the EOCs show that the methods converge with the correct order. The main mathematical techniques employed in this analysis of the stationary patterns is the Turing instability theory. This paper addresses the question of how population diffusion affects the formation of the spatial patterns in the Gray-Scott model by Turing mechanisms. In particular, we present a theoretical analysis of results of the numerical simulations in two dimensions. We have observed the formation of spatial patterns during the evolution, which are sparsely isolated ordered spot patterns that emerge in space. In this research we focuse on three areas: first, the analytical analysis; second, the numerical analysis and third, the application. We use these spatial patterns to understand the nature of population distribution and to understand the mechanism of interaction of the populations.

Received: 2 February 2014, Revised: 17 May 2014, Accepted: 16 June 2014.

Keywords: Pattern Formation, Turing instability, Gray-Scott model, Stability analysis.

Index to information contained in this paper

1. Introduction

Various spatial patterns have been observed in the physical world, such as stripe, spot, mixture of both patterns on animal skins; spiral waves in the Belousov-Zhabotinsky (BT) model, among many others. In 1952, Alan Turing [14] first pro-

*Corresponding author. Email: yau4real2006@yahoo.com

posed a simple mathematical model (reaction-diffusion system) to describe chemical reaction and diffusion to account for morphogenesis, that is, how patterns develope in biological systems. This study is the foundation of modern pattern formation. In [14], Turing employed linear stability analysis to determine the threshold for the instability of spatially homogeneous equilibrium solutions of general two components reaction diffusion models. Turings original work has stimulated numerous theoretical and numerical studies of reaction diffusion systems, which focus on pattern formation from a spatially uniform state that is near the transition from linear stability to linear instability. In 1993, Pearson [9] observed that for parameter values far from the Turing instability regime, the Gray-Scott model in a two-dimensional spatial domain can exhibit a rich variety of spatio-temporal patterns including, stationary spots, traveling spots, spot self-replication, spot-annihilation, growing stripes, labyrinthian patterns , stripe filaments, and spatial-temporal chaos, etc. The common feature in all of these patterns is that each consists of two distinct states of solutions: some localized regions where the chemical concentrations are very large, and a background ambient spatially homogeneous state. As time evolves, the localized regions of elevated chemical concentrations can remain stable, or develop very complicated structures through drifting, splitting, breaking, etc., driven by intricate and unknown mechanisms that depend on the range of parameters in the reaction-diffusion model.

The dynamics of spontaneous spatial pattern formation, first introduced to biology by Turing [14] five decades ago, has recently been attracting attention in many subfields of biology to describe various phenomena. Spatial modelling today is a leading scientific research area aiming at studying and understanding disease transmission in space [14]. We want to use the spatial epidemic models to investigate the dynamical behaviour of complex physical systems with relation to epidemic spread [13]. In modelling the dynamics of infectious diseases a particular important role is played by correct identification of the precise mechanism for a disease transmission [4].

In epidemiology, one of the central goals of mathematical epidemiology is to predict in populations how diseases transmit in space. For instance, the SARS epidemic spread through 12 countries within a few weeks. The classical epidemic SIR model describes the infection and recovery process in terms of three ordinary differential equations for susceptibles (S), infected (I) and recovered (R), which has been studied by many researchers [1–4, 6, 13] and the reference cited therein. These systems depend mainly on two parameters, the infection rate and the recovery rate. A growing body of work reports on the role of spatial patterns on evolutionary processes in the host population structure [5, 7, 9, 10]. Projections of the spatial spread of an epidemic and the interactions of human movement at multiple levels with a response protocol will facilitate the assessment of policy alternatives.

In the last several decades, chemical kinetics has produced a variety of phenomenon that have translated into challenging mathematical problems. A classical example is seen in the waves of the Belousov-Zhabotinskii reaction. Other examples have been produced that are not quite as complicated and require fewer species interactions, but still yield very interesting behavior. One aspect of these systems is that they do not involve thermal transfer as an essential part of the interaction. Since the 1950s, fundamental studies in reaction kinetics have focused on nonisothermal systems, i.e. where thermal feedback is a critical element. In 1968, Selkov described a particular autocatalytic model of glycolysis. The version of this model due to Gray and Scott is investigated below. Gray-Scott wanted to provide the same foundation for isothermal autocatalytic systems, i.e. chemical feedback. This model becomes the basis of our paper.

In the paper by Pearson [13], very complicated patterns were described for a parabolic system known as the Gray-Scott system. Pearson did a thorough numerical study of the system and found a complex structure in the solutions. However, Pearson used a simple integration scheme and left open the question regarding numerical artifacts. We are able to confirm the results from Pearson and show that more robust numerical schemes produce the same results. We also provide a bifurcation analysis giving the existence of non-uniform solutions for the steady state problem, i.e. the elliptic system of Gray-Scott.

2. The Schnakenberg Reaction

A well studied reaction-diffusion equation is the Schnakenberg system

$$\begin{cases} \dfrac{\partial S}{\partial t} - \nabla^2 S = \gamma(a - S + S^2 I) \\ \dfrac{\partial I}{\partial t} - d\nabla^2 I = \gamma(b - S^2 I)\,, \end{cases} \qquad \Omega\,, t > t_0 \tag{1}$$

for the pair $(S(\mathbf{x}, t), I(\mathbf{x}, t))$, some real numbers a, b and d and to be completed with appropriate initial conditions and boundary conditions. For concreteness, let us choose homogeneous Neumann boundary conditions on all the boundary.

It is easily shown that the steady state values of (1) are

$$S^* = a + b, \qquad I^* = \frac{b}{(a+b)^2}. \tag{2}$$

A detailed linear stability can be found in [6] and the following borrows their methods. Let $f(S, I)$ and $g(S, I)$ denote the RHS of the first and second equation in (1) respectively. Then in the absence of diffusion the system is linearly stable provided that

$$f_S + g_I < 0 \quad \text{and} \quad f_S g_I - f_I g_S > 0, \tag{3}$$

where the derivatives are evaluated at the equilibrium point. With the addition of diffusion the system can evolve to an inhomogeneous steady state. This phenomenon is known as diffusion driven instability, or Turing instability after the author who first described it in [14]. Let us consider a small perturbation from the equilibrium and write it as $\tilde{S} = S - S_c$ and $\tilde{I} = I - I_c$. Write $\boldsymbol{\psi} = (\tilde{S}, \tilde{I})$. Then linearising (1) we obtain

$$\frac{\partial \boldsymbol{\psi}}{\partial t} = \gamma \begin{pmatrix} f_S & f_I \\ g_S & g_I \end{pmatrix} \boldsymbol{\psi} + \begin{pmatrix} 1 & 0 \\ 0 & d \end{pmatrix} \nabla^2 \boldsymbol{\psi} \tag{4}$$

This can be solved by separation of variables to yield

$$\boldsymbol{\psi}(\mathbf{x}, t) = \sum_k \mathbf{c_k} e^{\lambda t} \psi_k, \tag{5}$$

where the ξ_k are the modes which solve the homogeneous Neumann problem

$$\nabla^2 \psi_k + k^2 \psi_k = 0. \tag{6}$$

These modes will decay with time unless their wavenumber k lies in the range

$$k_-^2 < k^2 < k_+^2, \tag{7}$$

where

$$k_\pm = \frac{\gamma}{2d}\left[df_S + g_I \pm \sqrt{(df_S + g_I)^2 - 4df_S g_I - f_I g_S}\right], \tag{8}$$

and the derivatives are evaluated at equilibrium. Thus if we perturb the system from equilibrium, under certain choices of parameters, we can expect exponential growth of some modes which correspond to the linearly unstable modes of (5).

3. Numerical Solution

Due to the non-linearity, an analytical solution to (1) is not readily available. Thus let us try to obtain a solution numerically, using the unit square as a simple domain. To discretise space we use the finite element method, and we shall experiment with a few time discretisation methods. The treatment of the non-linear terms were always explicit - here we shall consider ways to treat the non-linear terms implicitly thereby hopefully adding greater stability to the methods.

The choices $a = 0.1$, $b = 0.9$, $d = 10$ and $\gamma = 29$ will lead to diffusion driven instability. The eigenmodes of (6) have the form $\cos(n\pi x)\cos(m\pi y)$ for $n, m \in \mathbb{Z}$. The parameters chosen guarantee that the modes corresponding to $n^2 + m^2 = 1$ are linearly unstable.

Let T_h be a mesh of the 2D unit square and call each node $\mathbf{x}_i$. With each $\mathbf{x}_i$ associate the pyramid function ϕ_i which is one on $\mathbf{x}_i$ and zero everywhere else. Then $\{\phi_i\}$ spans the space of piecewise linear polynomials on T_h. Now, implementation of FEM yields

$$\begin{cases} (1+\gamma)\, M\dot{\mathbf{S}} + A\mathbf{S} - \gamma B(\mathbf{S},\mathbf{I})\mathbf{S} = \gamma a \mathbf{1}_\phi \\ M\dot{\mathbf{I}} + dA\mathbf{I} + \gamma B(\mathbf{S},\mathbf{S})\mathbf{I} = \gamma b \mathbf{1}_\phi \end{cases} \tag{9}$$

where the matrices A and M are the matrices with entries

$$a_{ij} = \int_\Omega \nabla\phi_i \cdot \nabla\phi_j \, d\mathbf{x}, \quad m_{ij} = \int_\Omega \phi_i \phi_j \, d\mathbf{x}. \tag{10}$$

$\mathbf{1}_\phi$ is the column matrix with j-th entry ϕ_j and, given some vectors $\mathbf{a}$ and $\mathbf{b}$, $B(\mathbf{a},\mathbf{b})$ is the matrix matrices with entries

$$B_{ij} = \sum_{k=1}^{N_h}\sum_{l=1}^{N_h} a_k b_l \int_\Omega \phi_k\phi_l\phi_i\phi_j \, d\mathbf{x}. \tag{11}$$

It is readily checked that given a third vector $\mathbf{c}$, the matrix B satisfies

$$B(\mathbf{a},\mathbf{b})\mathbf{c} = B(\mathbf{a},\mathbf{c})\mathbf{b} = B(\mathbf{c},\mathbf{b})\mathbf{a}. \tag{12}$$

Equation (9) does not yet lend itself to a numerical solution. First, it still continuous with respect to time. Second, the nonlinearity in the matrix B does not allow a solution to be gained by "simple" inversion. There are a number of ways

to discretise in time. We will consider the backward Euler, Crank-Nicholson, and the multi-step θ method. Define

$$\mathbf{G}_1(\mathbf{S},\mathbf{I}) = A\mathbf{S} + \gamma M\mathbf{S} - \gamma B(\mathbf{S},\mathbf{I})\mathbf{S} - \gamma a\mathbf{1}_\phi \tag{13}$$

$$\mathbf{G}_2(\mathbf{S},\mathbf{I}) = dA\mathbf{I} + \gamma B(\mathbf{S},\mathbf{S})\mathbf{I} - \gamma b\mathbf{1}_\phi \tag{14}$$

Using the uniform step size Δt, using the backward Euler method we solve at the $(n+1)$-th timestep

$$\begin{cases} \dfrac{\mathbf{S}^{n+1}-\mathbf{S}^n}{\Delta t} + \mathbf{G}_1(\mathbf{S}^{n+1},\mathbf{I}^{n+1}) = 0 \\ \dfrac{\mathbf{I}^{n+1}-\mathbf{I}^n}{\Delta t} + \mathbf{G}_2(\mathbf{S}^{n+1},\mathbf{I}^{n+1}) = 0 \end{cases} \tag{15}$$

The backward Euler is first order convergent. For Crank-Nicholson we solve

$$\begin{cases} \dfrac{\mathbf{S}^{n+1}-\mathbf{S}^n}{\Delta t} + \dfrac{1}{2}\left[\mathbf{G}_1(\mathbf{S}^{n+1},\mathbf{I}^{n+1} + \mathbf{G}_1(\mathbf{S}^n,\mathbf{I}^n)\right] = 0 \\ \dfrac{\mathbf{I}^{n+1}-\mathbf{I}^n}{\Delta t} + \dfrac{1}{2}\left[\mathbf{G}_2(\mathbf{S}^{n+1},\mathbf{I}^{n+1}) + \mathbf{G}_2(\mathbf{S}^n,\mathbf{I}^n)\right] = 0 \end{cases} \tag{16}$$

The Crank-Nicholson method is second order convergent.

In this problem it is natural to split the operators $\mathbf{G}_1$ and $\mathbf{G}_2$ into their linear and non-linear parts. The multistep θ-method divides each timestep into three unequal portions and allows us solve the linear and non-linear parts separately. Thus, we first solve

$$\begin{cases} \dfrac{\mathbf{S}^{n+\theta}-\mathbf{S}^n}{\theta\Delta t} + A\mathbf{S}^{n+\theta} + \gamma M\mathbf{S}^{n+\theta} = \gamma a\mathbf{1}_\phi + \gamma B(\mathbf{S}^n,\mathbf{I}^n)\mathbf{S}^n \\ \dfrac{\mathbf{I}^{n+\theta}-\mathbf{I}^n}{\theta\Delta t} + dA\mathbf{I}^{n+\theta} = \gamma b\mathbf{1}_\phi - \gamma B(\mathbf{S}^n,\mathbf{I}^n)\mathbf{S}^n \end{cases} \tag{17}$$

then

$$\begin{cases} \dfrac{\mathbf{S}^{n+1-\theta}-\mathbf{S}^{n+\theta}}{(1-2\theta)\Delta t} - \gamma B(\mathbf{S}^{n+1-\theta},\mathbf{I}^{n+1-\theta})\mathbf{S}^{n+1-\theta} = \gamma a\mathbf{1}_\phi - A\mathbf{S}^{n+\theta} - \gamma M\mathbf{S}^{n+\theta} \\ \dfrac{\mathbf{I}^{n+1-\theta}-\mathbf{I}^{n+\theta}}{(1-2\theta)\Delta t} + \gamma B(\mathbf{S}^{n+1-\theta},\mathbf{I}^{n+1-\theta})\mathbf{S}^{n+1-\theta} = \gamma b\mathbf{1}_\phi - dA\mathbf{S}^{n+\theta} \end{cases} \tag{18}$$

and finally

$$\begin{cases} \dfrac{\mathbf{S}^{n+1}-\mathbf{S}^{n+1-\theta}}{\theta\Delta t} + A\mathbf{S}^{n+1} + \gamma M\mathbf{S}^{n+1} = \gamma a\mathbf{1}_\phi + \gamma B(\mathbf{S}^{n+1-\theta},\mathbf{I}^{n+1-\theta})\mathbf{S}^{n+1-\theta} \\ \dfrac{\mathbf{I}^{n+1}-\mathbf{I}^{n+1-\theta}}{\theta\Delta t} + dA\mathbf{I}^{n+1} = \gamma b\mathbf{1}_\phi - \gamma B(\mathbf{S}^{n+1-\theta},\mathbf{I}^{n+1-\theta})\mathbf{S}^{n+1-\theta} \end{cases} \tag{19}$$

The first and third step the non-linear term is treated explicitly and the linear terms implicitly, whilst in the second step it is the other way around. For $\theta = 1 - \frac{1}{\sqrt{2}}$ this method is second order convergent.

To deal with the non-linearity, we shall use Picard iteration and the Newton-Raphson method which are both iterative techniques. For ease, we shall illustrate

their use on the backward Euler formula (15) only. At the $(n+1)$-th timestep, the $(k+1)$-th Picard iterate of (15) is the solution of

$$\begin{cases} \left[\left(\frac{1}{\Delta t}+\gamma\right)M + A - \gamma B(\mathbf{S}_k^{n+1}, \mathbf{I}_k^{n+1})\right]\mathbf{S}_{k+1}^{n+1} = \gamma a \mathbf{1}_\phi + \frac{1}{\Delta t} M\mathbf{S}^n \\ \left[\frac{1}{\Delta t} M + dA + \gamma B(\mathbf{S}_k^{n+1}, \mathbf{S}_k^{n+1})\right]\mathbf{I}_{k+1}^{n+1} = \gamma b \mathbf{1}_\phi + \frac{1}{\Delta t} M\mathbf{I}^n \end{cases}. \tag{20}$$

Alternatively, we may use the Newton-Raphson method. Taking everything to the RHS of (15), define

$$\mathbf{F}_1(\mathbf{S}^{n+1}, \mathbf{I}^{n+1}) = \left[\left(\frac{1}{\Delta t}+\gamma\right)M + A - \gamma B(\mathbf{S}^{n+1}, \mathbf{I}^{n+1})\right]\mathbf{S}^{n+1} - \gamma a \mathbf{1}_\phi - \frac{1}{\Delta t} M\mathbf{S}^n \tag{21}$$

$$\mathbf{F}_2(\mathbf{S}^{n+1}, \mathbf{I}^{n+1}) = \left[\frac{1}{\Delta t} M + dA + \gamma B(\mathbf{S}^{n+1}, \mathbf{S}^{n+1})\right]\mathbf{I}^{n+1} - \gamma b \mathbf{1}_\phi - \frac{1}{\Delta t} M\mathbf{I}^n\,. \tag{22}$$

The $(k+1)$-th Newton-Raphson iterate is the solution of

$$J_{\mathbf{F}_i}(\mathbf{S}_k^{n+1}, \mathbf{I}_k^{n+1})\left(\mathbf{S}_{k+1}^{n+1} - \mathbf{S}_k^{n+1}, \mathbf{I}_{k+1}^{n+1} - \mathbf{I}_k^{n+1}\right) = -\mathbf{F}_i(\mathbf{S}_k^{n+1}, \mathbf{I}_k^{n+1}) \quad i = 1, 2\,, \tag{23}$$

where $J_{\mathbf{F}_i}$ is the Jacobian matrix and the column vector $\left(\mathbf{S}_{k+1}^{n+1} - \mathbf{S}_k^{n+1}, \mathbf{I}_{k+1}^{n+1} - \mathbf{I}_k^{n+1}\right)$ is understood to be the vertical concatenation of the first and second arguements. Using property (12) of the matrix B we have for some vector $\boldsymbol{\xi}$ the derivative

$$\begin{aligned} \frac{\partial \mathbf{F}_1(\mathbf{S}_k^{n+1}, \mathbf{I}_k^{n+1})}{\partial \mathbf{S}^{n+1}}\boldsymbol{\xi} &:= \lim_{h\to 0} \frac{\mathbf{F}_1(\mathbf{S}_k^{n+1} + h\boldsymbol{\xi}, \mathbf{I}_k^{n+1}) - \mathbf{F}_1(\mathbf{S}_k^{n+1}, \mathbf{I}_k^{n+1})}{h} \\ &= \left[\left(\frac{1}{\Delta t}+\gamma\right)M + A - 2\gamma B(\mathbf{S}_k^{n+1}, \mathbf{I}_k^{n+1})\right]\boldsymbol{\xi} \end{aligned} \tag{24}$$

Similarly we have,

$$\frac{\partial \mathbf{F}_1(\mathbf{S}_k^{n+1}, \mathbf{I}_k^{n+1})}{\partial \mathbf{I}^{n+1}}\boldsymbol{\xi} = -\gamma B(\mathbf{S}_k^{n+1}, \boldsymbol{S}_k^{n+1})\boldsymbol{\xi} \tag{25}$$

$$\frac{\partial \mathbf{F}_2(\mathbf{S}_k^{n+1}, \mathbf{I}_k^{n+1})}{\partial \mathbf{S}^{n+1}}\boldsymbol{\xi} = 2\gamma B(\mathbf{S}_k^{n+1}, \mathbf{I}_k^{n+1})\boldsymbol{\xi} \tag{26}$$

$$\frac{\partial \mathbf{F}_2(\mathbf{S}_k^{n+1}, \mathbf{I}_k^{n+1})}{\partial \mathbf{I}^{n+1}}\boldsymbol{\xi} = \left[\frac{1}{\Delta t} M + dA + \gamma B(\mathbf{S}_k^{n+1}, \mathbf{S}_k^{n+1})\right]\boldsymbol{\xi}. \tag{27}$$

Thus, at the $(n+1)$-th timestep the $(k+1)$-th Newton iterate (23) is the solution

of the system

$$\left[\left(\frac{1}{\Delta t}+\gamma\right)M + A - 2\gamma B(\mathbf{S}_k^{n+1},\mathbf{I}_k^{n+1})\right]\mathbf{S}_{k+1}^{n+1} - \gamma B(\mathbf{S}_k^{n+1},\mathbf{S}_k^{n+1})\mathbf{I}_{k+1}^{n+1} = -2\gamma B(\mathbf{S}_k^{n+1},\mathbf{I}_k^{n+1})\mathbf{S}_k^{n+1} + \gamma a\mathbf{1}_\phi + \frac{1}{\Delta t}M\mathbf{S}^n \tag{28a}$$

$$\left[\frac{1}{\Delta t}M + dA + \gamma B(\mathbf{S}_k^{n+1},\mathbf{S}_k^{n+1})\right]\mathbf{I}_{k+1}^{n+1} + 2\gamma B(\mathbf{S}_k^{n+1},\mathbf{I}_k^{n+1})\mathbf{S}_{k+1}^{n+1} = 2\gamma B(\mathbf{S}_k^{n+1},\mathbf{S}_k^{n+1})\mathbf{I}_k^{n+1} + \gamma b\mathbf{1}_\phi + \frac{1}{\Delta t}M\mathbf{I}^n\,. \tag{28b}$$

We expect the system to reach a spatially inhomogeneous steady state which suggests a suitable stopping criterion to be

$$\frac{||S^{n+1}-S^n||_2}{\Delta t} \quad \text{and} \quad \frac{||I^{n+1}-I^n||_2}{\Delta t} \leqslant \epsilon, \tag{29}$$

for some small number ϵ and where $||\cdot||$ denotes the L_2 norm.

Noteworthy: The matrix B is not a sparse matrix, it is a full matrix and it contributes more to the error of the discrete solution. But with the scheme described above, we can reduce the error by refining the discrete solution and adapting the time step and Newton-Raphson to linearize the terms the constitute the matrix B. If we don't do the above, the matrix B may cause instability and may cause convergence problems.

Experimental Order of Convergence

Define

$$\phi(x,y,t) = \left(\frac{x^3}{3}-\frac{x^2}{2}\right)\left(\frac{y^3}{3}-\frac{y^2}{2}\right)\left(1+e^t\right). \tag{30}$$

Then $S = I = \phi$ does not satisfy the Shnackenberg system, but it is the exact solution to the modified equation

$$\begin{cases} \dfrac{\partial S}{\partial t} - \nabla^2 S - \gamma(-S+S^2I) = \phi_t - (\phi_{xx}+\phi_{yy}) - \gamma(-\phi+\phi^3) \\ \dfrac{\partial I}{\partial t} - d\nabla^2 I - \gamma(b-S^2I) = \phi_t - d(\phi_{xx}+\phi_{yy}) - \gamma\phi^3)\,, \end{cases} \quad \Omega\,, t > t_0 \tag{31}$$

with homogeneous Neumann conditions and initial condition

$$S_0 = I_0 = 2\left(\frac{x^3}{3}-\frac{x^2}{2}\right)\left(\frac{y^3}{3}-\frac{y^2}{2}\right). \tag{32}$$

It is easily seen that the both variables tend to the inhomogeneous steady $\frac{u_0}{2}$.

If we now solve (31) using our different time-step methods we can calculate the error from the exact solution ϕ at each timestep. This was done using five different timesteps $(\Delta t)_i = 2^{-i}$, $i = 1, 2, 3, 4, 5$ for the time interval $t \in [0, 5]$.

A measure of the error from the exact solution at the $(n+1)$-th timestep is given by

$$S_{err}^{n+1} = ||S^{n+1} - \phi(t = t^{n+1})||_2, \tag{33}$$

and a measure of the total error committed for a particular timestep is given by

$$S_{err,i} = \sum_m (\Delta t)_i \frac{S_{err}^{m+1} + S_{err}^m}{2}, \tag{34}$$

which is the area under the graph of a t-S_{err} plot. Similar quantities may be defined for the I variable.

If we approximate the error as $S_{err} \sim ce^{(\Delta t)_i}$, for some constant c, then we may approximate the order of convergence by

$$EOC = \frac{\log(S_{err,i}) - \log(S_{err,i-1})}{\log((\Delta t)_i) - \log((\Delta t)_{i-1})}, \quad i > 1. \tag{35}$$

Euler's method:

level	h	L^2-Error	L^2-EOC	L^∞-Error	L^∞-EOC
1.00000	0.50000	2.25086e-01	1.04378	1.12543e-01	0.93338
2.00000	0.25000	1.09179e-01	1.07624	2.72948e-02	0.96584
3.00000	0.12500	5.17796e-02	1.11317	6.47244e-03	1.00277
4.00000	0.06250	2.39366e-02	1.13786	1.49604e-03	1.04746
5.00000	0.03125	1.07278e-02	1.15294	3.35244e-04	1.10554
6.00000	0.01562	4.61824e-03	1.21863	7.21600e-05	1.11823
7.00000	0.00781	1.87737e-03	1.23246	1.46669e-05	1.13220
8.00000	0.00391	6.95563e-04	1.34018	2.71704e-06	1.19142
9.00000	0.00195	2.13815e-04	1.35597	4.17608e-07	1.21557

Table 1. The L^2, H^1, L^∞ errors and their EOCs for $\gamma = 10$, $a = 0.1$, $b = 0.9$, using backward Euler's scheme.

Crank Nicolson method:

level	h	L^2-Error	L^2-EOC	L^∞-Error	L^∞-EOC
1.00000	0.02500	1.12543e-02	2.04378	2.81358e-04	2.09333
2.00000	0.01250	5.45896e-03	2.07624	6.82370e-05	2.09658
3.00000	0.00625	2.58898e-03	2.11317	1.61811e-05	2.09977
4.00000	0.00313	1.19683e-03	2.15786	3.74009e-06	2.10446
5.00000	0.00156	5.36391e-04	2.16594	8.38111e-07	2.10554
6.00000	0.00078	2.30912e-04	2.18633	1.80400e-07	2.11823
7.00000	0.00039	9.38684e-05	2.19246	3.66674e-08	2.13220
8.00000	0.00020	3.47781e-05	2.19501	6.79260e-09	2.15914
9.00000	0.00010	5.06908e-06	2.19797	1.04402e-09	2.15255

Table 2. The L^2, L^∞ errors and their EOCs for $\gamma = 10$, $a = 0.1$, $b = 0.9$, using Crank-Nicolson scheme.

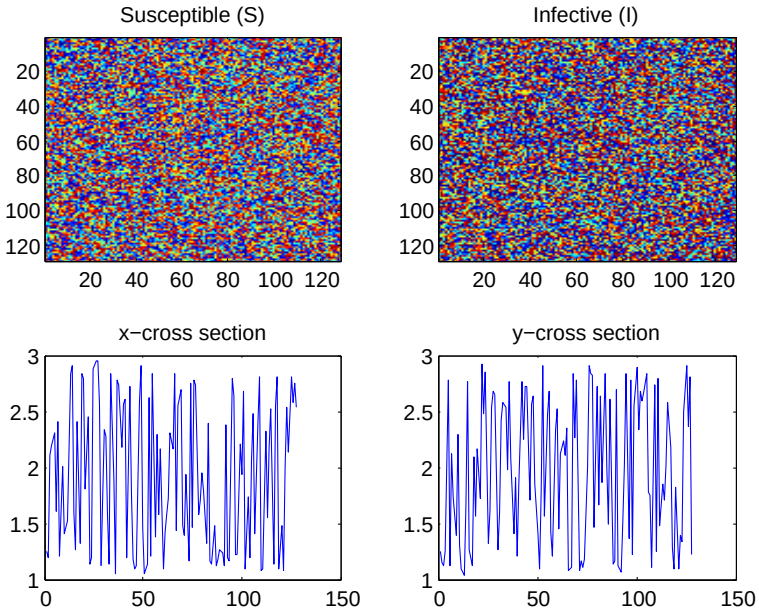

Figure 1. Time evolution corresponding to $\gamma = 10$, this is the initial solutions of 1 for $a = 0.1$, $b = 0.9$.

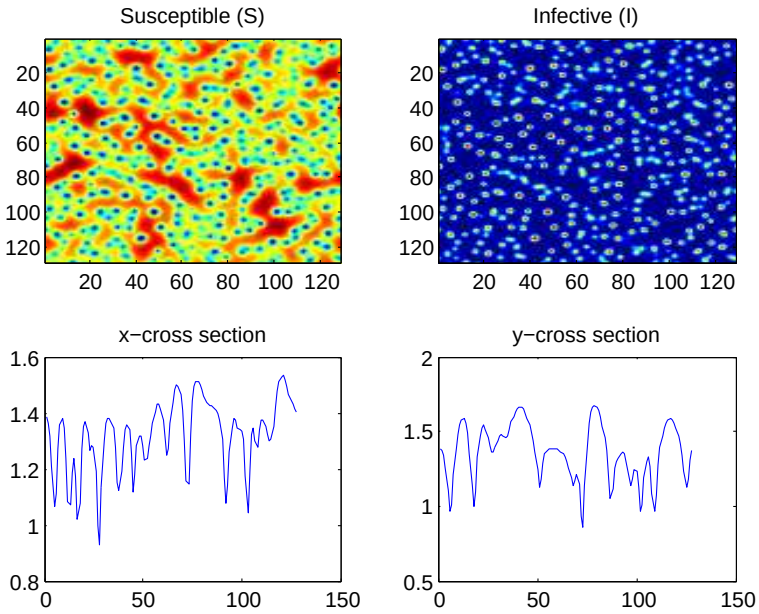

Figure 2. Time evolution corresponding to $\gamma = 20$, this shows sparse spotted pattern for $a = 0.1$, $b = 0.9$.

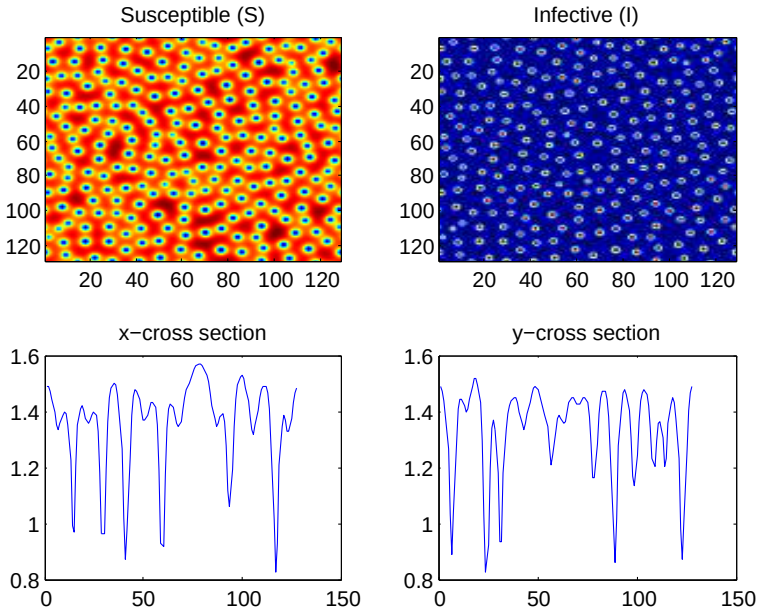

Figure 3. Time evolution corresponding to $\gamma = 50$, spotted pattern for the system 1 for $a = 0.1$, $b = 0.9$.

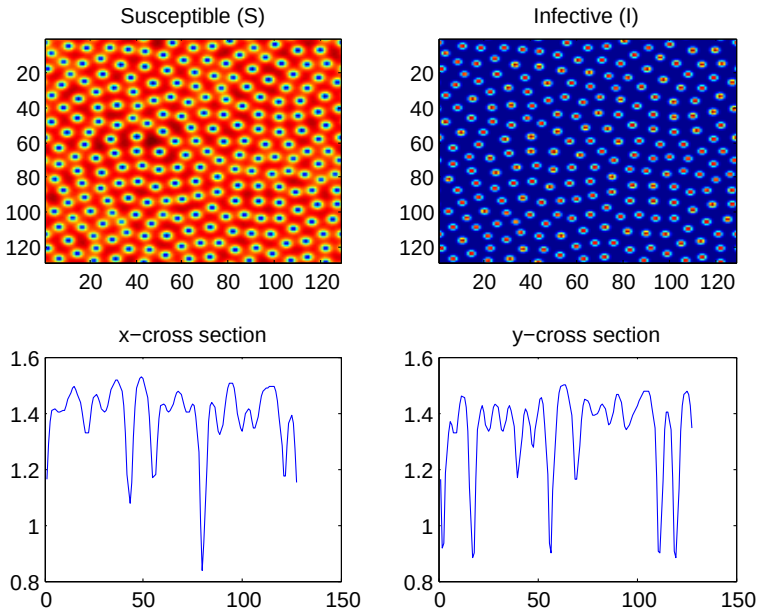

Figure 4. Time evolution corresponding to $\gamma = 100$, fully matured spot patterns of 1 for $a = 0.1$, $b = 0.9$.

The biological meaning of spot patterns can be varied depending on what is modelled. For instance, pattern formation from epidemic modelling can be described as follows. First, change in color from blue to red means from low concentrations (densities) to high concentrations (densities) of the population. Red spots (peaks) on blue background means the individuals are isolated zones and disconnected with high densities and the blue area which has low densities is larger to the red spots area. Therefore, from epidemic point of view this area is safe. In the other hand, blue spots (troughs) on a red background means the individuals are isolated zones with low densities and remaining area is of high densities which bigger than the spots area. This area is not safe.

4. Conclusions and Discusion

In this paper we have considered two numerical schemes for solving the Gray-Scott model. The non-linearity was handled implicitly using Newton-Raphson method. We presented the numerical results in tables 1 and 2. We computed the error in L^2 and L^∞ norms and the experimental order of convergence (EOC) for each scheme in the corresponding norms. The backward Euler converged with EOC of about one (order one convergence) and Crank-Nicolson converged with order two (EOC of about two) and this agreed well with the theory. The most important part of this paper are the combination of both analytical and numerical results and using two different numerical methods to solve the model. Both two methods showed interesting results, see tables 1 and 2 for details.

In the second part of this paper, we studied spatial patterns using the backward Euler's method. The Gray-Scott model 1 was investigated and was shown to generate spot patterns using implicit numerical methods and standard bifurcation analysis. Future work on these equations is directed at understanding the exact onset of the nonuniform solutions as a function of some bifurcation parameter. It would also be interesting to understand exactly how certain modes establish overall patterns and know how stable these are with respect to perturbations. We numerically solved the system using the above derived schemes in matlab. In this paper, we found spot patterns in the spatial Gray-Scott model driven by the diffusion. From the analysis of the Turing space and numerical simulations one can see that the attracting positive equilibrium will produce instability driven by the diffusion and the instability leads to the spot patterns within the Turing space. This may explain the prevalence of disease in large-scale geophysics. The positive equilibrium is stable in the non-spatial models, but it may lose its stability with respect to perturbations of certain wavenumbers and converge to heterogeneous distributions of populations.

References

[1] Beltrami. E, *Mathematics for dynamic modeling*, Academic Press, N.Y, (1989).
[2] Cross. M,*Notes on the Turing instability and chemical instabilities*, Lecture note, Beijing Normal University, (2006).
[3] Driessche. P. van den and Watmough. J, *Reproduction numbers and sub-threshold endemic equilibria for compartmental models of disease transmission*, Mathematical Biosciences, **180 (1)** (2002) 29–48.
[4] Liu. Q and Jin. Z, *Formation of spatial patterns in an epidemic model with constant removal rate of the infectives*, Journal of Statistical Mechanics: Theory and Experiment, P05002 **5** (2007).
[5] Murray. J. D., *Mathematical Biology*, Biomathematics. Springer-Verlag, New York, **19** (1993).
[6] Murray. J. D., *Mathematical Biology*, Springer, 3 edition, (2003).
[7] Ouyang. Q and Swinney. H. L., *Transition to chemical turbulence*, Chaos, **1(4)** (1991) 411–420.
[8] Parandin. N and Ezadi. S., *Application Neural Network to Solve Ordinary Differential Equations*, International Journal of Mathematical Modelling & Computations, **3(3)** (2013).
[9] Pearson. J. E., *Complex patterns in a simple system*, Science, **261** (1993) 189–192.

[10] Pierre. M and Schmitt. D., *Blowup in Reaction-Diffusion Systems with Dissipation of Mass*, SIAM, (2000).
[11] Robin. E., *Modelling Pattern Formation in Reaction-Diffusion Systems*, Master thesis, Copenhagen University, (1994).
[12] Singh. S, Dube. R and Singh. R., *Production Model with Selling Price Dependent Demand and Partial Backlogging Under Inflation*, International Journal of Mathematical Modelling & Computations, **1(1)** (2011).
[13] Sun. G., Jin. Z., Liu. Q and Li. L., *Pattern formation in a spatial S-I model with non-linear incidence rates*, Journal of Statistical Mechanics: Theory and Experiment, (2007).
[14] Turing. A. M., *The Chemical Basis of Morphogenesis*, Biological Sciences, Series B, Philosophical Transactions of the Royal Society of London, **52 (1)** (1990) 153-197.
[15] Yau. M. A., *On the stability and threshold analysis of an epidemic model*, International Journal of Mathematical Modelling & Computations, **3 (2)** (2013).